

# Soft-Clamped Perimeter Modes of Polygon Resonators

Zhihao Niu<sup>1,\*</sup> and Yuanyuan Zhao<sup>1,†</sup>

<sup>1</sup>Quantum Science Center of Guangdong-Hong Kong-Macao Greater Bay Area, Shenzhen 518045, China  
(Dated: June 24, 2025)

Polygon resonators are known for their small size and high force sensitivity. We propose an analytical model to predict the mechanical quality factors ( $Q$ ) of polygon perimeter modes by incorporating a stress term in the Timoshenko-Gere equation. We discuss the origin of losses and their relationship with polygon structure dimensions. Notably, we demonstrate that the torsion loss can be suppressed through the torsion angle of supporting tethers. These results offer new insights into optimizing high  $Q$  polygon resonators for cavity optomechanics, force sensing, and multimode physics of phononic structures.

*Introduction.* — Recent advancements have facilitated ultra-high quality factor ( $Q$ ) nanomechanical resonators, attributed to the phenomenon known as "dissipation dilution" [1, 2]. This phenomenon stems from the nonlinear stress-strain coupling, which gives rise to a quadratic relationship between the resonator's elongation and its vibration amplitude [3]. Notably, dissipation dilution significantly minimizes energy loss in the mechanical system through geometric engineering and stress enhancement, rather than relying solely on material optimizing [1, 3]. This opens up exciting avenues for device design.

Investigating the structural design and forces inherent in nanomechanical systems has revealed that the mode curvature at boundaries is a major source of the mechanical energy loss [1, 4]. Reducing the amplitude of the mechanical modes is an effective way to minimize the energy loss in these systems. Several innovative techniques, referred to as "soft clamping" [1], have been developed specifically for the clamping points to achieve the low-energy-loss. Previous studies have concentrated on tapered clamping [5], hierarchical structuring [6, 7], phononic bandgap engineering [8–10], and perimeter modes in polygon resonators [11].

Remarkably, the perimeter modes in polygon resonators have emerged as promising candidates for integrated quantum optomechanical systems [11]. In the tapered-clamping approach [5], enhancement of  $Q$  is challenging, as it is constrained to the material's yield stress-to-deposition stress ratio. In the hierarchical structuring approach [6, 7], the torsional losses in cascaded branchings hinder the resonators from attaining the "clampless" limit. Furthermore, in comparison to the phononic crystals (PnCs) [8–10], the fundamental perimeter modes of polygon structures [11] can reach a high-quality factor of  $3.6 \times 10^9$  with their tenfold reduced size. This compact structure is imperative for practical integration with optical microcavities, since submicron gaps are necessary for strong near-field optomechanical coupling [12]. Additionally, soft-clamping of PnCs is restricted to higher order modes. This will limit the applications on practical sensing, which favors the fundamental mode due

to its lower stiffness and cleaner spectral background. Importantly, soft-clamped perimeter modes in polygon resonators demonstrate exceptional frequency scalability, with a quality factor  $Q$  greater than  $10^8$ , maintained across more than four octaves (170 kHz – 2.5 MHz). Moreover, the  $Q$ s of the perimeter modes exhibit a high thermal-noise-limited force sensitivity of  $420 \text{ zN}\sqrt{\text{Hz}}$  at room temperature, which is comparable to that of atomic force microscopy cantilevers operating at millikelvin temperature ( $190 \text{ zN}\sqrt{\text{Hz}}$ ).

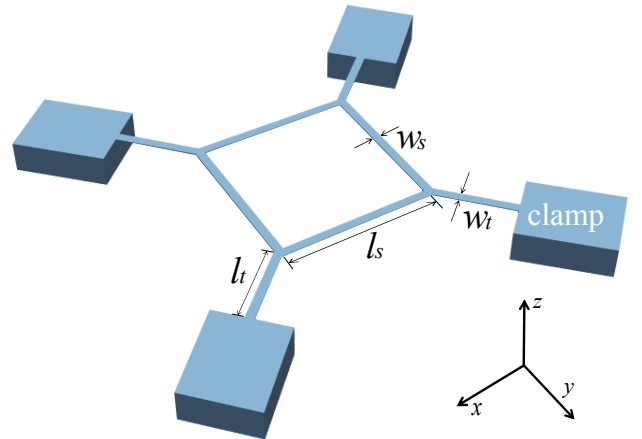


FIG. 1. Schematic representation of the polygon resonator (light blue) with index number  $N = 4$  and clamps (light blue). The substrates are represented in black.  $l_s$ ,  $l_t$ ,  $w_s$ ,  $w_t$  represent polygon side length, tether length, polygon side width, and tether width, respectively.

Perimeter modes are advantageous from the perspectives of engineering design and sensing applications. Nevertheless, the current model simulation, which can be matched with experiments and applications, remains relatively preliminary [11]. Consequently, we develop a comprehensive analytical framework that incorporates the tether torsion mode into the previous model analysis, and take into account the torsional resonance in the tethers. In the simulations and analysis, the polygon resonators are composed of a commercial material,

silicon nitride ( $\text{Si}_3\text{N}_4$ ). The detailed stress analysis is applied to the Timoshenko-Gere (TG) theory. The model displays remarkable predictive accuracy, with frequency estimations within 0.1% of FEM (finite element method) results across the entire operational range. Furthermore, our findings indicate that boundary losses are substantially amplified by the coupling between the polygon side bending modes and the tether torsional modes. Importantly, these losses can be tuned through adjusting the tether length, providing a flexible strategy for optimizing quality factors.

This letter is structured as follows. First, we start with two main sources of the dissipation loss in the polygon systems under the narrow-beam approximation. We then derive the vibration of polygon sides, and the supporting tethers, respectively. Consequently, the analytical dissipation dilution can be derived through the modified TG equations by the coupling of these two vibrations. Next, we calculate the  $Q$ 's of a sample  $\text{Si}_3\text{N}_4$  nanomechanical resonator through FEM and compare the results with our analytical results. We can accurately predict the resonant frequencies and the dissipation dilution factors of perimeter modes.

*Loss analysis.* — Dissipation dilution can be fundamentally understood through the interaction between a harmonic oscillator and a lossless potential [2]. The quality factor of a mechanical mode experiencing dissipation dilution can be enhanced due to

$$Q = D_Q \cdot Q_{\text{int}}. \quad (1)$$

Here,  $D_Q$  is the dissipation dilution factor and  $Q_{\text{int}}$  is the material's intrinsic quality factor inversely proportional to the material loss angle ( $Q_{\text{int}} = 1/\phi$ ) [13]. The dilution factor  $D_Q$  of the  $n^{\text{th}}$  perimeter mode adopts the general dissipation dilution form of the flexural modes of a stressed mechanical resonator [14]:

$$D_{Q,n} = \frac{\langle W_{\text{total}} \rangle}{\langle W_{\text{lossy}} \rangle} = \frac{1}{\alpha_n \lambda + \beta_n \lambda^2}, \quad (2)$$

with total stored energy  $\langle W_{\text{total}} \rangle$ , lossy part  $\langle W_{\text{lossy}} \rangle$ .  $\alpha_n$  and  $\beta_n$  are coefficients determined by the resonator's boundary curvature and the distributed bending over the rest of the mode, respectively. The strain parameter  $\lambda = \frac{h}{l} \sqrt{\frac{E}{12\sigma}}$  depends on the resonator length  $l$ , thickness  $h$ , Young's modulus  $E$ , and stress  $\sigma$ .

To study the soft-clamped modes in polygon resonators, we start with a four-interconnected beam structure as a general example, as illustrated in Fig. 1. Each beam is supported by two tethers, located at the vertices of the polygon resonator. According to the symmetry of the whole system, the displacement profile of the fundamental perimeter mode is illustrated with a degenerate symmetric vibration pattern in Fig. 2. The transverse

reaction forces on opposing tethers demonstrate phase cancellation, resulting in negligible net bending moments. However, the out-of-plane tangential displacement components generate a non-zero torque about the tether axes, inducing torsional dissipation.

In particular, as a result of the practical design considerations, the narrow-beam approximation is employed with  $l/w \gg 1$  for all constituent beams with length  $l$  and width  $w$  [11]. This justifies the zero boundary loss term ( $\alpha_n = 0$ ) in the dissipation kernel. Therefore, the dominant dissipation pathways in the polygon system originate from: (i) bending in the polygonal sides, and (ii) shear strain-induced dissipation in the supporting tethers. To analytically estimate the dissipation dilution factor of perimeter modes, we first derive the equations for the transverse displacement  $u(x)$  of the polygon sides, and the torsion angle  $\tau$  of the supporting tethers, respectively. Then we take their coupling into account.

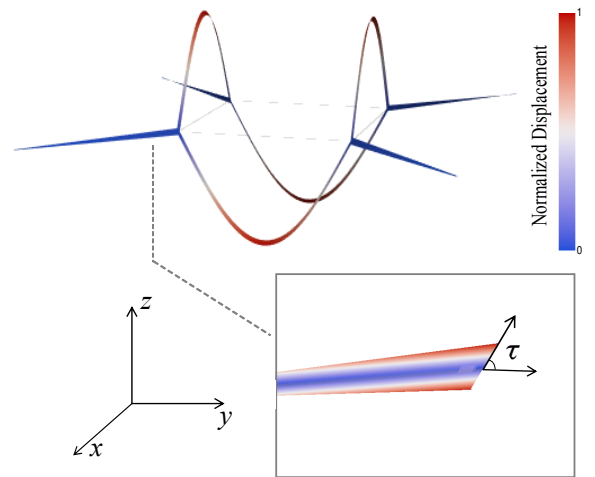


FIG. 2. FEM simulation of the fundamental mode of a stress preserving polygon resonator. The inset illustrates the torsion deformation caused by the out-of-plane displacement of two neighboring polygon sides.  $\tau$  is the torsion angle of the supporting tethers.

*Flexural dynamics of polygon sides.* — To model the bending-dominated dissipation, we analyze the transverse displacement field  $u(x)$  along each side of the  $N$ -sided polygon. Within the Euler-Bernoulli beam framework,  $u(x)$  follows the flexural string equation in the high tension limit [15]:

$$-\sigma_s(x) \frac{d^2 u}{dx^2} = \rho \omega_n^2 u. \quad (3)$$

where  $x$  is the axial coordinate along the polygon sides,  $\sigma_s$  the stress,  $\rho$  the material density, and  $\omega_n$  the degenerate symmetric frequency of the  $n^{\text{th}}$  flexural mode. The transverse displacement  $u(x)$  can be well approximated

by a sinusoidal profile  $u(x) = u_0 \sin(n\pi x/l_s)$  with polygon side length  $l_s$ . The degenerate symmetric frequency  $\omega_n$  can be determined by substituting  $u(x)$  into Eq. 3:

$$\omega_n^2 = \frac{\sigma_s n^2 \pi^2}{\rho l_s^2}. \quad (4)$$

*Torsional vibration of supporting tethers.* — The torsion angle  $\tau$  can be determined by the modified Timoshenko-Gere equation incorporating a stress term (see the supplementary material for the derivation of the modified TG equation):

$$EI_\psi \frac{\partial^4 \tau}{\partial x^4} + (\rho I_\psi \omega_n^2 - C - \sigma_t I_y) \frac{\partial^2 \tau}{\partial x^2} - \rho I_p \omega_n^2 \tau = 0. \quad (5)$$

where  $\sigma_t = \sigma_{xx}$  denotes the axial stress along the tether,  $x, y, z$  are the cartesian coordinates,  $I_p = \iint_A (y^2 + z^2) dA$  is the geometric moment of inertia,  $I_\psi = \iint_A \psi^2 dA$  ( $\psi \approx -yz$  the warping function [16]),  $A$  the cross section with thickness  $h$  and tether width  $w_t$ ,  $C$  the torsional rigidity ( $C = \iint_A G[(\frac{\partial \psi}{\partial y} - z)^2 + (\frac{\partial \psi}{\partial z} + y)^2] dA$ ), and  $G$  the shear modulus. We found that both Eq. 5 and the Euler-Bernoulli beam equation share the same structure and mode shape representation ([15] [p46], and Eq. S5). Consequently, the approximation method, used for high-stress conditions in Eq. 3, is equally applicable to Eq. 5, which can reduce to

$$-(C + \sigma_t I_y) \frac{d^2 \tau}{dx^2} = \rho I_p \omega_n^2 \tau, \quad (6)$$

where the axial stress  $\sigma_t$  contributes to the enhanced effective torsional rigidity of the tether through the term  $C + \sigma_t I_y$ . To solve Eq. 6, we assume a trial solution  $\tau(x) = \tau_0 \sin(kx + \phi_0)$  with the boundary condition  $\tau(0) = 0$ . The wave number  $k$  is found to be

$$k = \sqrt{I_p \sigma_s \frac{\pi^2}{l_s^2} \frac{1}{C + \sigma_t I_y}}. \quad (7)$$

*Coupling at the branch nodes.* — The flexural deformation of the polygon sides generates a torque that is directly coupled to the supporting tethers, initiating torsional wave propagation along the tether elements. The coupling between the transverse and torsional vibrations can be characterized by the following relation [7]:

$$u'(0) = \sin\left[\frac{(N-2)\pi}{2N}\right] \tau(x) = \cos\left(\frac{\pi}{N}\right) \tau_0 \sin(kl_t). \quad (8)$$

Here,  $l_t$  is the tether length. Eq. 8 demonstrates that the modal gradient at branch nodes  $u'(0)$  is determined by both the cosine of the polygon side number  $N$  and

$\sin(kl_t)$ . Since the system's tensile energy scales quadratically with  $u'(0)$ , theoretical  $Q$  maximization requires: (i) increasing the number of polygon sides, and (ii) achieving  $\sin(kl_t) = 1$ . However, the former has been shown to offer a limited practical improvement in dissipation dilution [6, 7]. Importantly, the latter provides a novel insight: when all material parameters except  $l_t$  are fixed (wave number  $k = \text{const}$ ), the modal gradient  $u'(0)$  - and consequently the dissipation dilution factor  $D_Q$  - can be tuned by adjusting  $l_t$ .

*Dissipation dilution factors and loss coefficient.* — The dissipation dilution factor  $D_Q$  of perimeter modes can be determined by estimating different energy components in Eq. 2. The "lossless" tensile energy is given by [7]

$$\langle W_{\text{tens}} \rangle = \frac{N}{2} \sigma_s w_s h \int_0^{l_s} [u'(x)]^2 dx. \quad (9)$$

where  $w_s$  is the polygon side width. The lossy energy comprises two components. The distributed bending energy along the polygon sides is

$$\langle W_{\text{bend}} \rangle = \frac{N}{2} \frac{E w_s h^3}{12} \int_0^{l_s} [u''(x)]^2 dx, \quad (10)$$

and the torsional lossy part is

$$\langle W_{\text{tors}} \rangle = N \frac{G w_t h^3}{12} \int_0^{l_t} (\tau'(x))^2 dx. \quad (11)$$

Substituting Eq. 9-11 into Eq. 2, and defining  $\lambda_l = \frac{h}{l_s} \sqrt{\frac{E}{12\sigma_s}}$  yield a dissipation dilution factor of

$$D_{Q,n}^{-1} = \frac{\langle W_{\text{bend}} \rangle + \langle W_{\text{tors}} \rangle}{\langle W_{\text{tens}} \rangle} = D_{Q,\text{bend}}^{-1} + D_{Q,\text{tors}}^{-1}. \quad (12)$$

with the two lossy contributions

$$D_{Q,\text{bend}}^{-1} = n^2 \pi^2 \lambda_l^2, \quad (13)$$

and

$$D_{Q,\text{tors}}^{-1} = \lambda_l^2 \frac{kl_s}{(1+\nu)r_w} \frac{2kl_t + \sin 2kl_t}{\cos^2(\pi/N) \sin^2(kl_t)}. \quad (14)$$

The first term in Eq. 12 is due to the distributed bending across the polygon sides, and sets a higher bound on the dissipation dilution factor. The second term depends on  $\lambda_l^2$  and is related to the torsional deformation of the supporting tethers. Notably, the term  $\sin^2(kl_t)$  in Eq. 14 implies that the dissipation dilution factor  $D_{Q,n}$  has a lower bound 0 when  $kl_t$  is an integer multiple of  $\pi$ . In

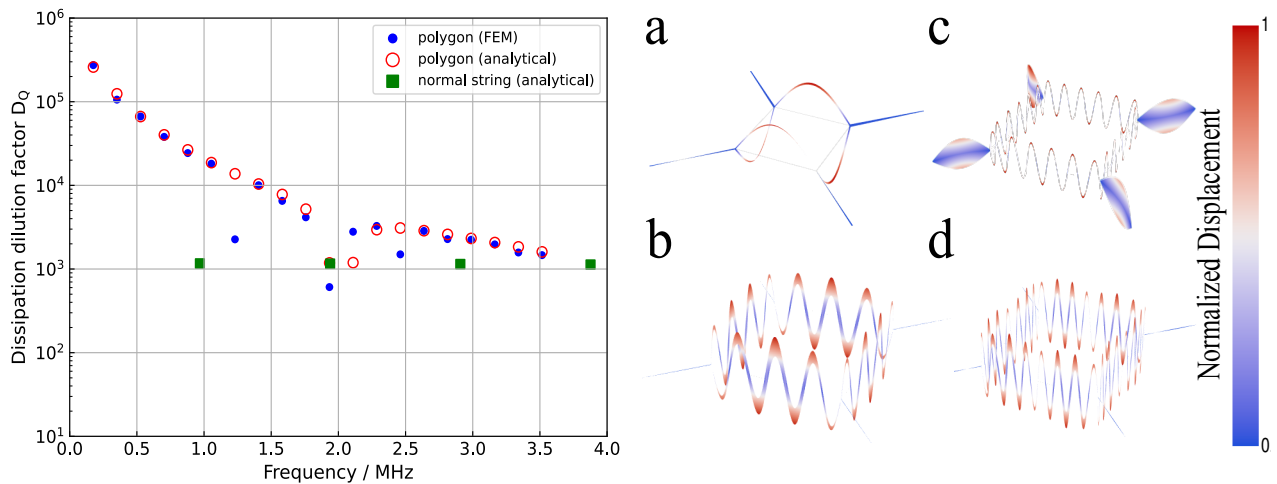


FIG. 3. Dissipation dilution factors and frequencies of the perimeter modes of the resonator with dimensions shown in the simulation part. Blue filled circles and red open circles correspond to FEM results and analytical results, respectively. Green squares correspond to out-of-plane modes of normal strings with the same dimensions and mechanical properties as the polygon sides. The four insets show the fundamental perimeter mode (a), and higher order perimeter modes where bending-torsion coupling exists (b, c, and d).

this case, the polygon sides exhibit zero transverse displacement, resulting in a system where the total energy manifests exclusively as dissipative torsional energy. To achieve the optimal dilution factor,  $l_t$  should be chosen to ensure  $kl_t = \pi/2$ .

*Simulation.* — As an illustrative case, we consider a polygon resonator characterized by the following geometric parameters: vertex count  $N = 4$ , side length  $l_s = 1400 \mu\text{m}$ , polygon side width  $w_s = 300 \text{nm}$ , support length  $l_t = 700 \mu\text{m}$ , and support width  $w_t = 400 \text{nm}$ . The resonator structure is made of a 100 nm commercial silicon nitride thin film with Young's modulus  $E = 250 \text{GPa}$ , mass density  $\rho = 3100 \text{kg/m}^3$ , Poisson's ratio  $\nu = 0.23$ , and deposition stress  $\sigma_0 = 1 \text{GPa}$ .

To demonstrate the precision of the theory model, we presented in Fig. 3 a comparative analysis of resonant frequencies and dissipation dilution factors for 20 modes of the polygon resonator, obtained through both the finite element method and analytical modeling. The results demonstrate that the analytical model achieves exceptional accuracy in predicting resonant frequencies, with relative errors below 0.1%. For most modes, the theoretically estimated dilution factors show quantitatively good agreement with FEM results. However, anomalies are observed in the 7th and 14th perimeter modes due to internal resonance effects, where energy transfers from primary flexural modes to coupled torsional modes (comparison between Insets 1, 3 and 4 reveals distinct torsional features). This leads to significant  $Q$ -factor degradation in primary modes [17]. Furthermore, the 11th and 12th mode exhibit deviation from theoretical predictions owing to bending-torsion mode coupling in the tethers. Remarkably, the dilution factor of the fun-

damental mode shows an approximately two orders of magnitude enhancement compared to that of a simple doubly-clamped beam of identical dimensions.

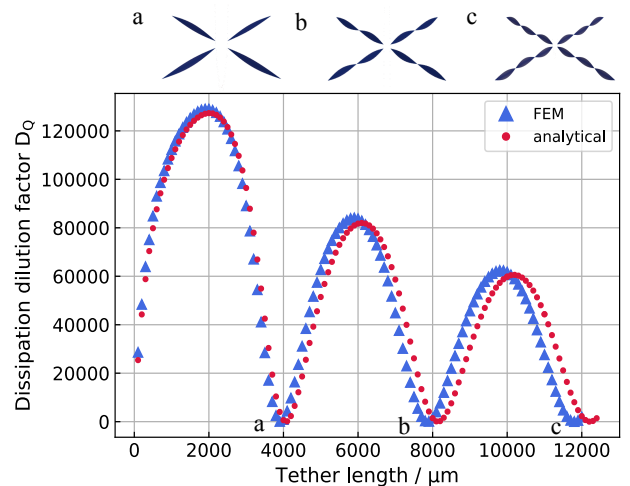


FIG. 4. Dissipation dilution factor  $D_Q$  for different tether lengths. blue dots and orange dots in d represent FEM simulation and theory model presented in this paper, respectively. The fundamental, second order, and third order modes are presented in Inset a, b, and c, corresponding to the lowest blue dots from left to right.

To investigate the hybridization between the bending modes of the polygon sides and the torsional modes of the tethers, we set  $l_s = 700 \mu\text{m}$  and varied the length of the tethers while keeping all other parameters constant. Fig. 4 plots the dissipation dilution factor as a function of the tether length in the polygon resonator, revealing three well-defined resonant peaks. The initial

peak exhibits the maximum dissipation dilution, while subsequent peaks display a progressive reduction in magnitude. This behavior originates from the torsional angle at the tether-polygon junction modulating the transverse displacement derivative of the polygon side - a quantity whose squared value directly governs the tensile energy based on Eq. 8. Crucially, the observed first peak position occurs at  $kl_t \approx \pi/2$ , whereas the trough coincides with  $kl_t \approx \pi$ , consistent with the theoretical model according to Eq. 14. These results confirm that tailored adjustment of tether length permits precise control over the quality factors of the resonator and offers valuable guidance to optimize high-performance polygon resonators. As the tether length increases, we also noticed that the peak positions predicted by the analytical model exhibit a growing deviation from the FEM simulations. This physical mechanism underlying the increase in  $k$  with  $l_t$  remains under investigation.

*Torsional dissipation dilution limit.* — An important issue in the study of polygon structures involves the enhancement of dissipative dilution in the supporting tethers. This phenomenon has been demonstrated in doubly-clamped stressed nanoribbons, similar to that of supporting tethers in polygon structures (see the supplementary material for a detailed derivation). Thus, if only the tethers are considered in a polygon structure system, the dissipation factor for the  $n^{\text{th}}$  torsional mode of the tethers can be expressed as follows:

$$D_{Q,t,n} \approx 1 + \frac{1}{\frac{2G}{\sigma_t} \frac{h^2}{w_t^2} + \frac{n^2 \pi^2}{12} \frac{Eh^2}{\sigma_t l_t^2} + \frac{h}{l_t} \sqrt{\frac{E}{3\sigma_t}}}. \quad (15)$$

The dimensions of the tethers ( $l_t \gg w_t$ ) and material properties of the silicon nitride film (see the simulation part) suggest that the first term  $\frac{2G}{\sigma_t} \frac{h^2}{w_t^2}$  in the denominator in Eq. 15 governs energy dissipation. This finding aligns with prior work [18] and reflects a limited torsional dissipation dilution.

*Conclusions and outlook.* — In this work, we present a comprehensive analytical study of perimeter vibrational modes in polygonal resonators. We derive the Timoshenko-Gere equation under the high tension condition for the angular displacement of nanoribbons. The modified equation is extended to the torsional vibration of supporting tethers of polygon resonators and accurately predict both the resonant frequencies and dissipation dilution factors of perimeter modes. The quality factor of the fundamental mode enhances by two orders of magnitude compared to uniform strings of the same dimensions. Moreover, our analysis reveals that the resonance of the tethers can significantly degrade the dissipation dilution factor of the perimeter mode, and the tether length can be used to tune the dilution factor. Our findings provide critical insights for designing high- $Q$  polygon resonators, with direct applications in

cavity optomechanics [19]. Additionally, our work impacts nanoscale force sensing [20, 21], enabling precision measurements in weak-force detection. Furthermore, our work advances the study of multimode phononic structures [22–24], offering new avenues for exploring topological phononics and non-Hermitian wave control.

## ACKNOWLEDGEMENTS

Y. Z. acknowledges the support from the National Natural Science Foundation of China (Grant No. 12474153, Grant No. 11804163), Guangdong Provincial Quantum Science Strategic Initiative (GDZX2401001).

\* niuzhihao@quantumsc.cn

† zhaoyuanyuan@quantumsc.cn

- [1] Y. e. a. Tsaturyan, Nature Nanotechnology **12**, 776 (2017).
- [2] G. González, Classical and Quantum Gravity **17**, 4409 (2000).
- [3] S. A. Fedorov, N. J. Engelsen, A. H. Ghadimi, M. J. Beryhi, R. Schilling, D. J. Wilson, and T. J. Kippenberg, Physical Review B **99**, 054107 (2019).
- [4] P.-L. Yu, T. Purdy, and C. Regal, Physical review letters **108**, 083603 (2012).
- [5] M. J. Beryhi, A. Beccari, S. A. Fedorov, A. H. Ghadimi, R. Schilling, D. J. Wilson, N. J. Engelsen, and T. J. Kippenberg, Nano letters **19**, 2329 (2019).
- [6] M. J. Beryhi, A. Beccari, R. Groth, S. A. Fedorov, A. Arabmoheghi, T. J. Kippenberg, and N. J. Engelsen, Nature Communications **13**, 3097 (2022).
- [7] S. A. Fedorov, A. Beccari, N. J. Engelsen, and T. J. Kippenberg, Physical review letters **124**, 025502 (2020).
- [8] A. Cupertino, D. Shin, L. Guo, P. G. Steeneken, M. A. Bessa, and R. A. Norte, Nature Communications **15**, 4255 (2024).
- [9] A. Beccari, D. A. Visani, S. A. Fedorov, M. J. Beryhi, V. Boureau, N. J. Engelsen, and T. J. Kippenberg, Nature Physics **18**, 436 (2022).
- [10] A. H. e. a. Ghadimi, Science **360**, 764 (2018).
- [11] M. J. Beryhi, A. Arabmoheghi, A. Beccari, S. A. Fedorov, G. Huang, T. J. Kippenberg, and N. J. Engelsen, Physical Review X **12**, 021036 (2022).
- [12] J. Guo, R. Norte, and S. Gröblacher, Physical review letters **123**, 223602 (2019).
- [13] P. R. Saulson, Physical Review D **42**, 2437 (1990).
- [14] Q. P. Unterreithmeier, E. M. Weig, and J. P. Kotthaus, Physical Review Letters **102**, 147202 (2009).
- [15] S. Schmid, L. G. Villanueva, and M. L. Roukes, *Fundamentals of nanomechanical resonators*, Vol. 49 (Springer, 2016).
- [16] J. Chopin and R. T. Filho, Physical Review E **99**, 043002 (2019).
- [17] K. Asadi, J. Yeom, and H. Cho, Microsystems & nano-engineering **7**, 9 (2021).
- [18] J. R. Pratt, A. R. Agrawal, C. A. Condos, C. M. Pluchar, S. Schlamminger, and D. J. Wilson, Physical Review X **13**, 011018 (2023).

- [19] M. Aspelmeyer, T. J. Kippenberg, and F. Marquardt, *Reviews of Modern Physics* **86**, 1391 (2014).
- [20] J. Moser, J. Güttinger, A. Eichler, M. J. Esplandiu, D. Liu, M. Dykman, and A. Bachtold, *Nature nanotechnology* **8**, 493 (2013).
- [21] E. Gavartin, P. Verlot, and T. J. Kippenberg, *Nature nanotechnology* **7**, 509 (2012).
- [22] T. Faust, J. Rieger, M. J. Seitner, P. Krenn, J. P. Kotthaus, and E. M. Weig, *Physical review letters* **109**, 037205 (2012).
- [23] V. Peano, C. Brendel, M. Schmidt, and F. Marquardt, *Physical Review X* **5**, 031011 (2015).
- [24] J. Lu, C. Qiu, L. Ye, X. Fan, M. Ke, F. Zhang, and Z. Liu, *Nature Physics* **13**, 369 (2017).